Simulation of a Charged Al2O3 Film As An Assisting Passivation Layer For a-Si Passivated Contact p-Type Silicon Solar Cells

Tian Pu (sherlock.pu@outlook.com)
Nanjing University of Aeronautics and Astronautics https://orcid.org/0000-0002-9428-2656
Honglie Shen
Nanjing University of Aeronautics and Astronautics https://orcid.org/0000-0002-2759-9880
Quntao Tang
Nanjing University of Aeronautics and Astronautics

Research Article

Keywords: Simulation, charged Al2O3 layer, a-Si passivated contact p-type silicon solar cell, HIT solar cell

Posted Date: February 23rd, 2021

DOI: https://doi.org/10.21203/rs.3.rs-215611/v1

Version of Record: A version of this preprint was published at Silicon on April 19th, 2021. See the published version at https://doi.org/10.1007/s12633-021-01105-4.

Abstract

In this paper, a charged Al_2O_3 tunneling film as an assisting for amorphous Si (a-Si) passivated contact layer is proposed and theoretically simulated for its potential application in improving a-Si passivated contact p-type (a-PC-p) solar cell. The concept is based on an Ag/n^+ c-Si/p c-Si/Al_2O_3/p^+ a-Si/Al structure. The key feature is the introduction of a charged Al_2O_3 layer, which facilitates the tunneling of holes through an Al_2O_3 insulator layer accompanied by the reduction of interface defect density (D_{it}). The negative charge in the Al_2O_3 layer makes the energy band of p-type c-Si bend upward, realizing the accumulation of holes and repelling of electrons at the c-Si/a-Si interface simultaneously. The influence of interface negative charges (Q_{it}) between a-Si and c-Si, Al_2O_3 thickness, Al_2O_3 bandgap, interface defect density (D_{it}) at the a-Si/c-Si interface are systematically investigated on the output parameters of a-PC-p cells. Inserting a charged Al_2O_3 film between the c-Si/a-Si interface, a +4.2 % relative efficiency gain is predicted theoretically compared with the a-PC-p cells without the Al_2O_3 layer. Subsequently, the device performance under various temperatures is simulated, and the insertion of a charged Al_2O_3 layer obviously decreases the P_{max} temperature coefficient from -0.336 % /℃ to -0.247 % /℃, which is analogous to that of Heterojunction with Intrinsic Thin layer (HIT) solar cell. The above results demonstrate a better temperature response for a-PC-p cells with a charged Al_2O_3 layer, paving a road for its potential application in high-efficiency and high thermal stability a-PC-p solar cells.

Highlights

- A charged Al_2O_3 assisting passivation layer is proposed for a-Si PC-p
- The Al_2O_3 layer makes the selective carrier tunneling at the c-Si/a-Si interface.
- A +4.2 % relative efficiency gain is predicted theoretically by the Al_2O_3
- The insertion of the Al_2O_3 layer reduces the P_{max} temperature coefficient greatly.

1. Introduction

In the last several years, the a-Si/c-Si passivated contact (a-PC) solar cell has attracted a large amount of attention due to its prominent high V_{oc} and higher efficiency. A famous example of the a-PC solar cell is the heterojunction technology (HJT) solar cell which achieves very high conversion efficiency by using hydrogenated amorphous silicon (a-Si:H) layer to effectively passivate the amorphous and crystalline silicon (c-Si) interface as well as at the metal contact area[1]. Compared with traditional diffusion processed homo-junction solar cells, the most attractive advantages of the a-PC solar cell are its lower deposition temperature (< 200 ℃) and better cell temperature coefficient (-0.25 %)[2]. As is known to all, the device quality is mainly determined by factors including a-Si emitter quality and interface quality between a-Si and c-Si. Defect states at the a-Si/c-Si interface could induce strong interface recombination in an a-PC solar cell if the interface defect density is larger than 1×10^{13} $cm^{-2}\cdot eV^{-1}$. The mid-gap with a low

interface state can be achieved by the insertion of intrinsic hydrogenated amorphous silicon. However, the narrow process window for depositing intrinsic hydrogenated amorphous silicon makes it very easy to grow epitaxially on the c-Si substrate[3]. The detrimental effect of an epitaxially grown interface normally causes a V_{oc} of a-PC solar cell lower than 600 mV. The defects in the epitaxial film are determined by the energy position within the bandgap and the capture cross-section of the electron and hole. Usually, an abruptness of the a-Si/c-Si interface without any initial epitaxial growth is more preferred. Therefore, a tunnel oxide insulator layer (usually SiO_2), is adopted to prohibit the epitaxial phenomenon and reduce recombination at the interface[4-5]. Generally speaking, the used SiO_2 should be as thin as possible to ensure the tunneling process (< 20 Å), while the interface passivation effect will be better if a thicker oxide layer is adopted. As a result, a trade-off between the tunneling process and interface passivation should be considered.

Generally speaking, a solar cell is based on a semiconductor material that absorbs light and then generates excess electrons and holes. The different types of contacts in a solar cell not only conduce to collect the different charge carriers but also serve as a semipermeable membrane so that one contact supports electrons getting across and blocks holes, while the other contact is exactly the opposite. Except being carrier-selective, the contacts are better to passivate the surface defects to ensure that the minority carriers are collected before their recombination. Such contacts can therefore be defined as contact passivation[6]. Recently, there has been an increasing interest in the application of tunneling layers for passivation contact in single-junction silicon-based solar cells. The used a-Si stack layer in HIT solar cells [7] and SiO_2/polycrystalline silicon stack layer[8] in high-efficiency n-type silicon solar cells are all, in fact, contact passivation structures. Therefore, the contact passivation structure is usually made of an ultrathin insulator layer and a highly doped semiconductor layer. The used insulator materials can be positively charged layers, i.e., a-SiN_x: H[9] and thermal SiO_2[10], which can lead to an effective surface passivation result on lightly doped n- or p-type substrate, as well as some negatively charged layer such as Al_2O_3[11]. Negative charges in Al_2O_3 are particularly suited to passivate the backside of the p-type solar cell. It is expected that the negative charges in Al_2O_3 can repel electrons and accumulate holes at the interface between a-Si and c-Si, which increases the probability of tunneling through the Al_2O_3 layer. Aluminum oxide (Al_2O_3) has potentially been used as an optional passivation material to standard a-SiN_x: H. The application of Al_2O_3 here could be summarized by two important trends. First, the photovoltaic (PV) industry has recently transferred the Al-back surface field (Al-BSF) cell to a dielectrically rear passivated cell[12-14]. This rear side passivated structure leads to a lower surface recombination loss, better light reflection inside the cell, and less suffered wafer bow for thinner wafers[15-17]. A passivated rear side is believed necessary for higher conversion efficiency and the possibility of thinner Si wafers application. Though the ultrathin SiO_2 layer has been widely used in a-PC solar cells, the use of an ultrathin Al_2O_3 layer as a tunnel oxide layer in contact passivation structure is rarely reported. Therefore, it is necessary for understanding how the parameters affecting tunneling, for example, the negative

charges (Q_{it}) in the a-Si and c-Si interface, Al_2O_3 thickness, interface defect density (D_{it}) between a-Si and c-Si.

In this paper, a p-type c-Si substrate a-Si passivated contact solar cell based on Ag/n^+ c-Si/p c-Si/Al_2O_3/p^+ a-Si/Al structure has been developed to study the variation of Q_{it} between a-Si and c-Si, Al_2O_3 thickness, Al_2O_3 bandgap and D_{it} at the a-Si/c-Si interface on a-PC cell performance using AFORS-HET software. The purpose of this paper is to investigate the influence of the charged Al_2O_3 layer on a-PC cell's performance, so the reference cell is not optimized.

2. Simulation Models

2.1. Tunneling theory

As direct quantum tunneling, the calculation of electron tunnel current $J_{e,tun}$ is based on the Tsu–Esaki equation[18] in semiconductor-insulator-semiconductor (SIS) structures:

$$J_{e,tun} = \frac{4\pi q m^*}{h^3} \int_{E_{min}}^{+\infty} T(E)N(E)\,dE \qquad (1)$$

where q is the elementary charge, E_{min} is the minimum conduction band edge energy to have tunneling effect, m^* is the tunneling effective mass and h is Planck's constant. The barrier transparency T(E) gives the probability of an electron with the energy E through the barrier to the tunnel.

With known effective masses for silicon, the result outside the integration sign is a constant. As a result, the tunneling current is dominated by the quasi-Fermi levels, the energy of the charge carriers and the transmission coefficient. This coefficient is the ratio of the outgoing compare with incoming flux, is found using the transfer matrix method to solve the Schrödinger equation. The major parameters are the height of the energy barrier, the mass of the tunneling effect and the thickness of the oxide.

2.2. Simulation parameters

We use the 1D simulation software "Automat FOR Simulation of HETerostructure" (AFORS-HET) developed at the Helmholtz Zentrum Berlin[19] to perform the numerical simulation in this case. AFORS-HET could solve one-dimensional semiconductor equations related to Shockley–Reed–Hall statistics. It utilizes an optical model based on the Lambert-Beer law for calculating the optical parameters. In this article's simulation, we assumed that the metal contacts are a flat band and the solar radiation AM 1.5 with a power density of 100 mW/cm^2 is introduced as a light source. The gap statistics of various types of a-Si:H layers and c-Si wafer are defined as a default value in the AFORS-HET configuration. Simulated cell structure with the position of the different layers is presented in **Fig.1**. The layer's given parameters are presented in **Table 1**.

Table 1 Input parameters used in the present simulation

Parameters	c-Si (n^+)	c-Si (p)	ALD Al_2O_3	a-Si:H (p^+)
Layer thickness (cm)	3.0×10^{-5}	0.018	Variable	5×10^{-7}
Dielectric constant	11.9	11.9	6	11.9
Electron affinity (eV)	4.05	4.05	2.5	3.9
Bandgap (eV)	1.12	1.12	Variable	1.72
Effective conduction band density (cm^{-3})	8.95×10^{18}	2.8×10^{19}		1.0×10^{20}
Effective valence band density (cm^{-3})	8.44×10^{18}	2.8×10^{19}		1.0×10^{20}
Electron mobility (cm^2/Vs)	119.5	1041		20
Hole mobility (cm^2/Vs)	159.9	413		5
Acceptor doping concentration (cm^{-3})	0	1.5×10^{16}		1.0×10^{20}
Donor doping concentration (cm^{-3})	10^{19}	0		0
Thermal velocity of electrons (cm/s)	1.0×10^{7}	1.0×10^{7}		1.0×10^{7}
Thermal velocity of holes (cm/s)	1.0×10^{7}	1.0×10^{7}		1.0×10^{7}
Layer density (g/cm^3)	2.328	2.328		2.328
Auger recombination coefficient for electron (cm^6/s)	0	2.2×10^{-31}		0
Auger recombination coefficient for electron (cm^6/s)	0	9.9×10^{-32}		0
Direct band-to-band recombination coefficient (cm^3/s)	9.5×10^{-15}	9.5×10^{-15}		0
fixed charge density (cm^{-2})			Variable	

At the rear side hetero-interface, defects are considered using a 1 nm thick highly defective c-Si interfacial layer which contains two Gaussian distributed density of states (DOS)[20]. The Gaussian distributions of donor-like and the acceptor-like have their maximum at 0.56 eV and 0.76 eV above the valence band (E_v). The standard deviation of both distributions is 0.2 eV and the electron and holes capture cross-sections (σ_e, σ_h) are 1×10^{-14} cm^{-2}. Their heights are adjusted to the equivalent interface defect densities (cm^{-2}), which is yield targeted.

Regarding the carrier transport mechanism, we assume drift-diffusion for c-Si/c-Si (homo-interfaces) and consider tunneling thermionic emission for c-Si/a-Si:H (hetero-interfaces). Here we should also consider a high doping level of the added a-Si layer will induce the bandgap narrowing.

The electrical current through the two semiconductors' interface is virtually the current that would flow through a fictitious insulating layer by tunneling in this simulation using AFROS-HET software. The conduction mechanism in this simulated structure could be explained as a hole tunneling from the valence band of the base p-type c-Si through the Al_2O_3 layer, then into the p^+ a-Si:H layer. The effective mass of bulk Al_2O_3 is 3-10 m_0, while an effective mass of 0.33 m_0 has been found for tunnel thin layers[21]. So the input effective mass of Al_2O_3 is set to 0.33 m_0. Bulk Al_2O_3 in the crystalline phase has a

bandgap of about 8.8 eV. For the atomic layer deposition deposited amorphous Al_2O_3 layer has a bandgap of about 6.4 eV[22]. This has been used unless stated otherwise. The dielectric constant and electron affinity values of the ultrathin Al_2O_3 layer are set according to the results reported in the literature [22].

3. Results And Discussion

Along with the introduction of Aluminum oxide (Al_2O_3) comes the introduction of atomic layer deposition (ALD) in the photovoltaic industry. ALD is different from conventional plasma-enhanced chemical vapor deposition tools due to the strict separation of the process gases in two half-cycles during deposition, resulting in a self-limited layer-by-layer growth. The strength of ALD is precisely thickness control and very good deposition uniformity over large area surfaces. Generally speaking, the excellent passivation performance of ALD Al_2O_3 originates from the combination of low D_{it} (chemical passivation) and high Q_{it} (field-effect passivation)[23]. The as-deposited thermal ALD Al_2O_3 usually possesses a relatively low D_{it} accompanied with a low value of Q_{it} while the as-deposited plasma ALD provides high D_{it} and high Q_{it}. With extra annealing treatment, both ALD processes show lower $D_{it} \leq 1\times10^{11}$ cm^{-2}[24-25]. Regarding the field-effect passivation, the thermal ALD-based Al_2O_3 film exhibits especially low Q_{it} of the order of 10^{11} cm^{-2} before annealing comparing to plasma ALD with Q_{it} of the order of 10^{12} cm^{-2}. Also, the highest Q_{it} value for plasma ALD can reach 10^{13} cm^{-2}[26-28] after annealing. Therefore, for the ALD Al_2O_3 film, Q_{it} can be adjusted from 1×10^{10}~10^{13} cm^{-2} by choosing different ALD processes and post-annealing treatment. To investigate the influence of Q_{it} at p-type c-Si/ALD Al_2O_3 interface on simulated a-PC-p cell's output parameters, Q_{it} is adjusted from 1×10^{10}~10^{13} cm^{-2} with D_{it} fixed at 10^{11} cm^{-2}. **Fig.2** presents the simulated a-PC-p cell's output parameters versus Q_{it}. It is seen that the cell's performance is enhanced with increasing Q_{it} from 10^{10} cm^{-2} to 10^{13} cm^{-2}. In the low Q_{it} (< 10^{12} cm^{-2}) region, the amount of Q_{it} is not enough to assist hole tunneling through the Al_2O_3 layer, as a result of which low J_{sc} and low FF appear. When Q_{it} increases from 10^{12} cm^{-2} to 10^{13} cm^{-2}, J_{sc} and efficiency increase while FF rarely changes. Therefore, it is suspected that enough amount of Q_{it} can ensure the tunneling process even though a dielectric layer is used. This is consistent with the result reported in the literature[28].

As the ALD Al_2O_3 layer thickness can influence the tunneling of carriers, various levels of Al_2O_3 layer thickness are adopted to study its effect on simulated a-PC-p cell's output parameters (shown in **Fig.3**). To understand how Q_{it} affects the Al_2O_3 layer of different thicknesses, Al_2O_3 layers of various thicknesses with and without Q_{it} are introduced (shown in **Fig.3**). For the Al_2O_3 layer without Q_{it}, the cell's FF decreases rapidly from 80.89 % to 49.33 % with Al_2O_3 thickness increasing from 0.2 nm to 0.4 nm. And FF, J_{sc} and efficiency are reduced to 40.66 %, 0.32 mA/cm^{-2} and 0.087 %, respectively, when Al_2O_3 thickness further increases to 1 nm. However, for the Al_2O_3 layer with -10^{13} cm^{-2} Q_{it}, both FF and efficiency of the cell rarely change even when increasing Al_2O_3 thickness to 1 nm. This demonstrates the

vital role Q_{it} plays in carrier tunneling. When Al_2O_3 thickness exceeds 1 nm, the cell with -10^{13} cm^{-2} Q_{it} loses its J_{sc} and efficiency rapidly, while its FF still rarely changes. Theoretically, the thicker the Al_2O_3 layer is, the lower the tunneling probability (T(E)) for carriers will be. Therefore, a thinner Al_2O_3 is desired for a high tunneling current. Besides, the added Q_{it} facilitates the alignment of the energy bands for both c-Si and a-Si, and causes the accumulation of holes at their interface, which results in a higher built-in potential. Therefore, the enhanced built-in potential facilitates the tunneling of holes through the barrier.

According to the simulated results shown in **Fig.2** and **Fig.3**, Q_{it} at the c-Si/a-Si interface have a significant influence on carrier transport through the Al_2O_3 dielectric layer. Q_{it} can maintain the successful tunneling of carriers without degrading the cell's performance. To figure out how Q_{it} influences the transport of carriers through the Al_2O_3 dielectric layer, band diagram and carrier distribution with the position of two different cells are calculated and compared. The Al_2O_3 dielectric layer thickness for both cells is fixed at 1 nm. The only difference between the two cells is that one cell has a Q_{it} of -10^{13} cm^{-2}, while the other has a Q_{it} of 0 cm^{-2}. As shown in **Fig.4** (a) and (b), the band diagram of the cell with a Q_{it} of -10^{13} cm^{-2} bends upward compared to the other cell, indicating that the high Q_{it} leads to an accumulation of holes at the interface. **Fig.4** (c) shows the density of electron and hole at the c-Si/a-Si interface, a large number of holes with an order of 10^{13} cm^{-3} accumulated on the c-Si side accompanied by a smaller amount of electrons for the cell with a Q_{it} of 10^{13} cm^{-2}. Cell with a Q_{it} of 0 only has a much smaller amount of electrons and holes on the c-Si side. This reveals the fact that Q_{it} can influence the carrier distribution at the c-Si/a-Si interface and thus the selective transport of carriers through the dielectric layer. Based on the above three figures, a schematic band diagram illustrating how the charged Al_2O_3 layer affecting the transport behavior of electrons and holes is shown in **Fig.4** (d). As can be seen, the charged Al_2O_3 layer behaves like a filter which can allow the transport of holes through it with repelling electrons backward.

The oxide bandgap (E_g) can also affect the magnitude of the effect caused by the charges. A difference in the bandgap of Al_2O_3 has been figured for different deposition processes, there is a variation from 6.2 eV to 7.0 eV was found in the literature[29,30]. In **Fig.5**, the simulated a-PC-p cell's four output parameters as a function of the Al_2O_3 bandgap are shown for Q_{if} value of -$10^{13}$$cm^{-2}$. The cell's efficiency is mainly influenced by the change of J_{sc} and FF. When E_g is less than 6.7eV, the decrease of efficiency along with increasing E_g is due to the decrease of FF. However, when E_g is bigger than 6.7eV, the loss of efficiency is mostly determined by the decrease of J_{sc}. It is expected that the barrier height at the c-Si/a-Si interface can be modeled by choosing the Al_2O_3 layer of different E_g. Therefore, selecting a bigger E_g Al_2O_3 layer means higher barrier height at the c-Si/a-Si interface, which results in a relatively low tunneling probability, and thus a low FF and a low J_{sc}.

We know that the interface defect density (D_{it}) has a great influence on c-Si/a-Si interface recombination. The distribution of D_{it} at the c-Si/a-Si interface is a state's superposition near band edges and states.

These states include surface pretreatment-induced strain bonds, bonds between adsorbates, dangling bonds, and atoms of different oxide layers leading to several groups of interface states. The minimum value for these interface state distributions can be considered as a measurement of the electronic quality of the wafer and interface. **Fig.6** shows the dependence of simulated a-PC-p cells' output parameters on D_{it}. As can be seen, the output parameters of a-PC-p cells, whether with or without the charged Al_2O_3 layer, tend to decrease with increasing D_{it}. When D_{it} is less than 1×10^{13} cm^{-2}, the a-PC-p cell with charged Al_2O_3 layer possesses a higher efficiency than that without charged Al_2O_3 layer. However, the tendency operates in the opposite way when D_{it} is over 1×10^{13} cm^{-2}, indicating that the D_{it} can have different effects on cell efficiency for different cells in different D_{it} regions. As is known to all, D_{it} at the a-Si/c-Si interface is more than 1×10^{13} cm^{-2} and the Al_2O_3 layer can supply a certain extent of interface passivation. Therefore, the a-PC-p cell's efficiency can be improved by inserting charged Al_2O_3 at the a-Si/c-Si interface. Compared with directly deposited a-Si on the c-Si surface, the presence of the charged Al_2O_3 can reduce D_{it} and thus higher efficiency can be obtained.

Fig.7 (a) shows a comparison of the I-V characteristics of a simulated cell with only a-Si and with a-Si plus Al_2O_3 at c-Si/p^+ a-Si interface, assuming a fixed interface charge density (Q_{it}) of -1×10^{13} cm^{-2}. The simulation shows that there is a large efficiency gain (4.2 % relative) when changing from a pure a-Si to a-Si plus Al_2O_3 (Q_{it} = -1×10^{13} cm^{-2}) at the c-Si/Al interface. Notably, there is a change of the I-V parameters of the solar cells, i.e., not only an improvement in V_{oc} and J_{sc}, but also a reduction in FF (see in the inset table in **Fig.7** (a)). V_{oc} is improved by reducing the interface recombination within the hole collecting region. Compared with pure p^+ a-Si, the addition of a charged Al_2O_3 layer can reduce a partial portion of D_{it} by saturating some dangling bonds at the c-Si/p^+ a-Si interface (D_{it} is reduced from 10^{13} cm^{-2} to 10^{11} cm^{-2}). A relative J_{sc} boost of 5.4 % is observed for the cell with the Al_2O_3 layer. Comparing the spectral response of simulated cell with only a-Si and with a-Si plus Al_2O_3 at c-Si/p^+ a-Si interface, it is seen that the external quantum efficiency (EQE) increase from 800 nm to 1100 nm (seen in **Fig.7** (b)), which is the absorption region of the backside. Below 800 nm, the spectral response is almost the same. In the wavelength region from 800 nm to 1000 nm, EQE increases. As the front side is the same for both cells, the change of EQE between 800 ~ 1000 nm must be due to the insertion of the Al_2O_3 layer at the c-Si/p^+ a-Si interface. It is expected as light in this region is mostly absorbed in the 180 μm thick p-type base, Q_{it} increases built-in potential at c-Si/p^+ a-Si interface which ultimately boosts the number of holes collected at the cell's backside. This can mostly stem from the enhanced interface passivation effect due to the Al_2O_3 layer. Though a relative FF decrease of 3.0 % occurs, which may be due to the insertion of 1 nm Al_2O_3 layer, a high FF still maintains in comparison to the Al_2O_3 layer without Q_{it} (as discussed in **Fig.3**). As discussed before, the cell with the Al_2O_3 layer and Q_{it} has a higher built-in potential, and thus enhances hole collection which leads to a relatively high FF.

To evaluate the device performance under various temperatures, the temperature response of the a-PC-p cells with and without charged Al_2O_3 layer is shown in **Fig.8**, where the efficiency can also represent the

maximum output power. The temperature dependences of V_{oc}, J_{sc}, FF and efficiency are illustrated by **Fig.8** (a)-(d), respectively. As the temperature increases from 26.85 ℃ to 76.85 ℃, J_{sc} is enhanced; whereas both V_{oc} and efficiency drop; FF fluctuates as the temperature changes. Based on the simulated results, a linear fitting is adopted to calculate the temperature coefficients of V_{oc}, J_{sc}, FF and efficiency, respectively. The obtained temperature coefficients for both cells are listed in **Table** 2. As can be seen, the insertion of a charged Al_2O_3 layer drops the P_{max} temperature coefficient from -0.336 % / ℃ to -0.247 % / ℃, indicating that the output power degrades less with increasing working temperature. Simultaneously, the V_{oc} temperature coefficient also drops for the better interface passivation of charged Al_2O_3 layer. The above results demonstrated a better temperature response for the a-PC-p cell with a charged Al_2O_3 layer, paving a road for its potential application in high-efficiency and high thermal stability a-PC-p solar cells.

Table 2 Simulated temperature coefficients of V_{oc}, J_{sc}, FF and efficiency.

Sample	P_{max}	V_{oc}	J_{sc}
a-Si	-0.336%	-0.270%	+0.014%
a-Si + Al_2O_3 with -1×10^{13} cm^{-2} charges	-0.247%	-0.223%	+0.006%

4. Conclusions

In this study, we theoretically investigate the charged Al_2O_3 film as an assisting passivation layer in improving the performance of the p-type silicon-based a-Si passivated contact solar cell (Ag/n^+ c-Si/p c-Si/Al_2O_3/p^+ a-Si/Al structure). The purpose of the charged Al_2O_3 tunnel film is to realize the accumulation of holes and simultaneously to enhance the c-Si/a-Si interface passivation, which facilitates the tunneling of holes through the Al_2O_3 insulator layer and the reduction of interface defect density (D_{it}) respectively. Through the systematic optimization of interface negative charges (Q_{it}) between a-Si and c-Si, Al_2O_3 thickness, Al_2O_3 bandgap, and interface defect density (D_{it}) at a-Si/c-Si interface, a +4.2 % relative efficiency gain is predicted theoretically compared with the a-PC-p cell without Al_2O_3 layer. Based on the temperature-dependent investigation of output parameters of both a-PC-p cells, the decrease of the P_{max} temperature coefficient from -0.336 % /℃ to -0.247 % /℃ is observed by the insertion of a charged

Al_2O_3 layer. The above results demonstrate the better performance of a-PC-p cell with a charged Al_2O_3 layer, indicating its potential application in high-efficiency and high thermal stability a-PC-p solar cells.

Declarations

Funding statement

This work has been financially supported by the National Nature Science Foundation of China (61774084), the open project of Key Laboratory of Materials Preparation and Protection for Harsh Environment, Ministry of Industry and Information Technology (XCA20013-3) and the Special Scientific Innovation Fund of Sihong County (H201901).

Conflict of Interest

We declare that we have no financial and personal relationships with other people or organizations that can inappropriately influence our work, there is no professional or other personal interest of any nature or kind in any product, service and/or company that could be construed as influencing the position presented in, or the review of, the manuscript entitled.

Author contributions

Conceptualization, Tian Pu.; software, Quntao Tang.; formal analysis, Tian Pu.; investigation, Tian Pu., Quntao Tang; resources, Honglie Shen.; data curation, Quntao Tang; writing—original draft preparation, Tian Pu.; writing—review and editing, Quntao Tang., Honglie Shen.; visualization, Tian Pu.; project administration, Honglie Shen.; funding acquisition, Honglie Shen. All authors have read and agreed to the published version of the manuscript.

Availability of data and material

The datasets generated during and/or analysed during the current study are available from the corresponding author on reasonable request.

Compliance with ethical standards

Conflict of Interest: The authors declare that they have no conflict of interest.

Research involving human participants and/ or animals: Not applicable

Informed consent: Informed consent was obtained from all individual participants included in the study.

Consent to participate

Not applicable

Consent for Publication

Not applicable

References

1. Park H, Lee YJ, Park J et al (2018) Front and Back TCO Research Review of a-Si/c-Si Heterojunction with Intrinsic Thin Layer (HIT) Solar Cell[J]. Trans Electr Electron Mater 19:165–172
2. Haschke J, Dupré O, Boccard M et al (2018) Silicon heterojunction solar cells: Recent technological development and practical aspects - from lab to industry[J]. Solar Energy Materials Solar Cells 187(1):140–153
3. Balaji P, Dauksher WJ, Bowden SG et al (2020) Improving surface passivation on very thin substrates for high efficiency silicon heterojunction solar cells[J]. Sol Energy Mater Sol Cells 216:110715
4. Liu W, Meng F, Zhang X et al (2015) Evolution of native oxide layer at a-Si:H/c-Si interface and its influence on silicon heterojunction solar cell.[J]. Angew Chem 51(3):748–751
5. Choi S, Min KH, Jeong MS (2017) Structural evolution of tunneling oxide passivating contact upon thermal annealing[J]. Scientific reports 7(1):12853
6. Limodio G, Yang G, Ge H et al (2019) Front and rear contact Si solar cells combining high and low thermal budget Si passivating contacts[J]. Sol Energy Mater Sol Cells 194(1):28–35
7. Xiao S, Zhou J, Huang S et al. Highly textured conductive and transparent ZnO films for HIT solar cell applications[J]. Journal of Physics D Applied Physics, 2015, 48(30)
8. Morisset A, Cabal R, Grange B et al (2019) Highly passivating and blister-free hole selective poly-silicon based contact for large area crystalline silicon solar cells[J]. Sol Energy Mater Sol Cells 200(15):109912
9. Hintzsche LE, Fang CM, Marsman M et al (2015) Formation of a Positive Fixed Charge at c – Si (111)/a – $Si_3N_{3.5}$: H Interfaces[J]. Phys Rev Appl 3(6):064005
10. Liu W, Yang X, Kang J et al (2019) Polysilicon Passivating Contacts for Silicon Solar Cells: Interface Passivation and Carrier Transport Mechanism[J]. ACS Appl Energy Mater 2(7):4609–4617
11. Bansal A, Srivastava P, Singh BR (2015) On the surface passivation of c-silicon by RF sputtered Al_2O_3 for solar cell application[J]. J Mater Sci: Mater Electron 26(2):639–645
12. Blakers A (2019) Development of the PERC Solar Cell[J]. IEEE J Photovolt 9(3):629–635
13. Hsu CH, Cho YS, Wu WY,, et al (2019) Enhanced Si Passivation and PERC Solar Cell Efficiency by Atomic Layer Deposited Aluminum Oxide with Two-step Post Annealing[J]. Nanoscale Res Lett 14:139
14. Liu PK, Cheng YL, Wang L et al. Crystalline Silicon PERC Solar Cell with Ozonized AlOx Passivation Layer on the Rear Side[J]. International Journal of Photoenergy, 2020, 2020:6
15. Allen TG, Bullock J, Yang X (2019) Passivating contacts for crystalline silicon solar cells[J]. Nature Energy 4:914–928

16. Gakis GP, Vahlas C, Vergnes H et al (2019) Investigation of the initial deposition steps and the interfacial layer of Atomic Layer Deposited (ALD) Al2O3 on Si[J]. Appl Surf Sci 492:245–254
17. Ye F, Yuan N, Ding J et al (2015) The performance of thin industrial passivated emitter and rear contacts solar cells with homogeneous emitters[J]. J Renew Sustain Energy 7(1):013122
18. Schulman JN (1998) Extension of Tsu-Esaki model for effective mass effects in resonant tunneling[J]. Applied physics letters 72(22):2829–2831
19. Physics and Technology of Amorphous-Crystalline Heterostructure Silicon Solar Cells, edited by W. G. J. H. M. van Sark, L. Korte, and F. Roca (Springer Berlin, Heidelberg, 2012), Chap. 4
20. Huang R, Yu M, Yang Q et al (2020) Numerical simulation for optimization of an ultra-thin n-type WS2/p-type c-Si heterojunction solar cells[J]. Comput Mater Sci 178:109600
21. Vexler MI, Tyaginov SE, Shulekin AF (2005) Determination of the hole effective mass in thin silicon dioxide film by means of an analysis of characteristics of a MOS tunnel emitter transistor[J]. J Phys: Condens Matter 17(50):8057
22. Huang H, Modanese C, Sun S (2018) Effective passivation of p + and n + emitters using SiO2/Al2O3/SiNx stacks: Surface passivation mechanisms and application to industrial p-PERT bifacial Si solar cells [J]. Sol Energy Mater Sol Cells 186:356–364
23. Hoex B, Gielis JJH, Van de Sanden MCM et al (2008) On the c-Si surface passivation mechanism by the negative-charge-dielectric Al_2O_3[J]. J Appl Phys 104(11):113703
24. Li J, Wang Y, Wan F et al (2020) Passivation via atomic layer deposition Al2O3 for the performance enhancement of quantum dot photovoltaics[J]. Sol Energy Mater Sol Cells 209(1):110479
25. Lee CY, Deng S, Zhang T et al (2018) Evaluating the impact of thermal annealing on c-Si/Al2O3 interface: Correlating electronic properties to infrared absorption [J]. AIP Adv 8:075204
26. Hezel R, Jaeger K (1989) Low-temperature surface passivation of silicon for solar cells[J]. J Electrochem Soc 136(2):518–523
27. Banerjee S, Das MK (2021) A review of Al2O3 as surface passivation material with relevant process technologies on c-Si solar cell[J]. Opt Quant Electron 60:53
28. Li S, Yang N, Yuan X et al (2019) Plasma-induced damage and annealing repairing in ALD-Al2O3/PECVD-SiNx stack[J]. Mater Sci Semicond Process 100:214–219
29. Roy AM, Lin J, Saraswat KC. The effect of fixed charge in tunnel-barrier contacts for Fermi-level depinning in germanium[J]. Electron Device Letters, IEEE, 2012, 33(6): 761–763
30. Bersch E, Rangan S, Bartynski RA et al (2008) Band offsets of ultrathin high-κ oxide films with Si[J]. Physical review B 78(8):085114

Figures

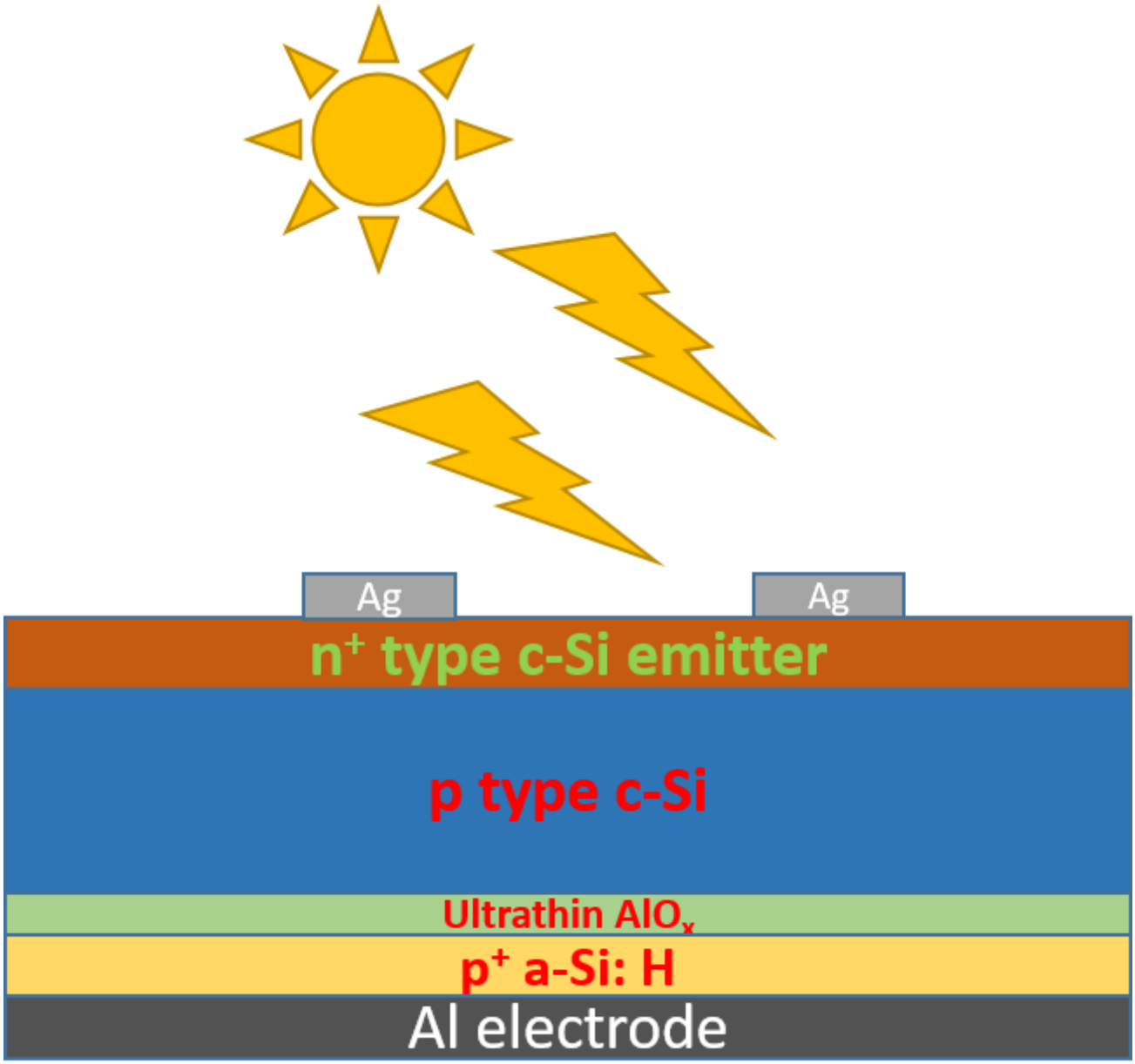

Figure 1

Schematic of simulated p-type HJ solar cell.

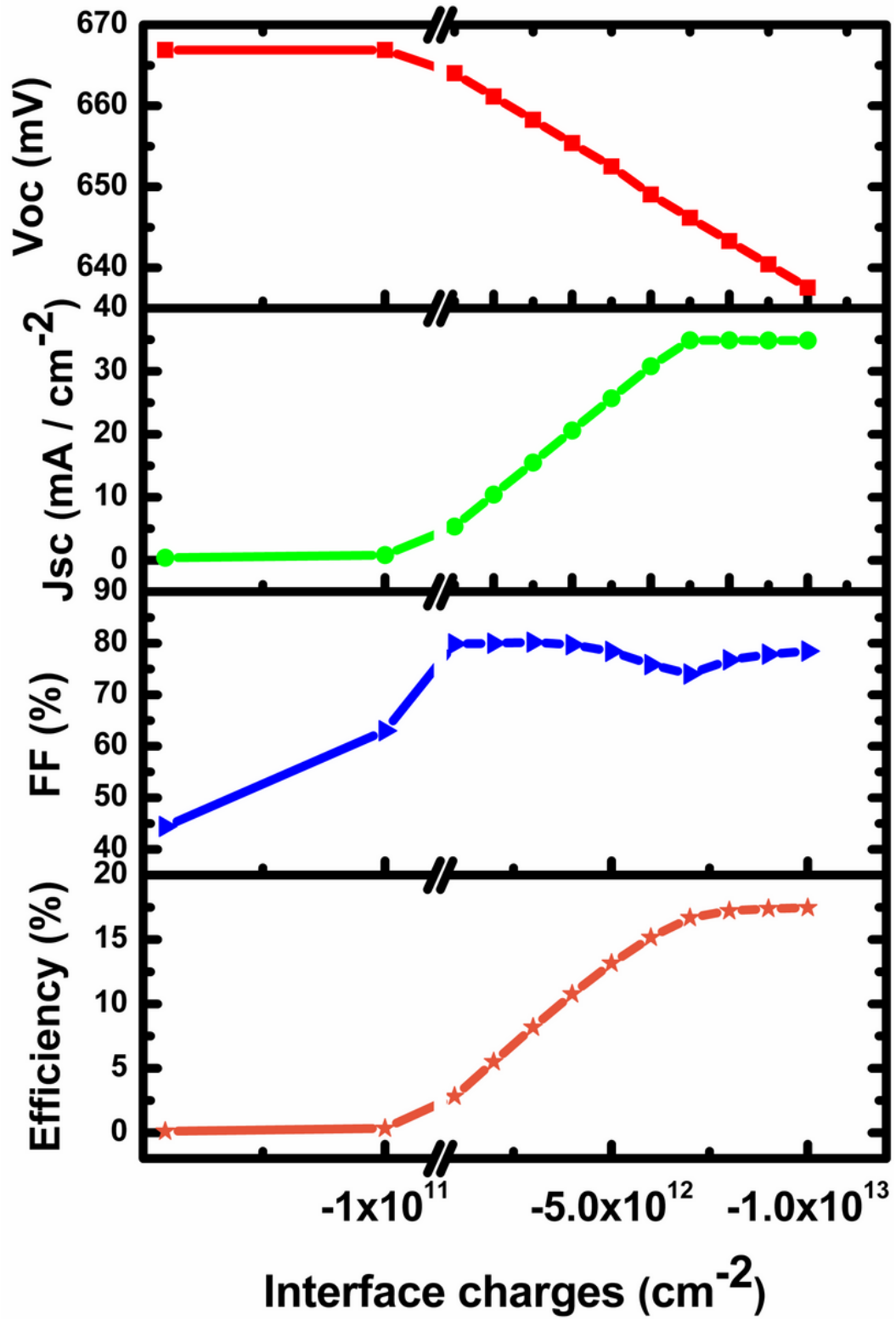

Figure 2

Output parameters of simulated HJ cell versus negative interface charges (Qit). Bandgap, Al2O3 thickness and interface defect density were fixed at 6.4 eV, 1 nm and 1011 cm-2, respectively.

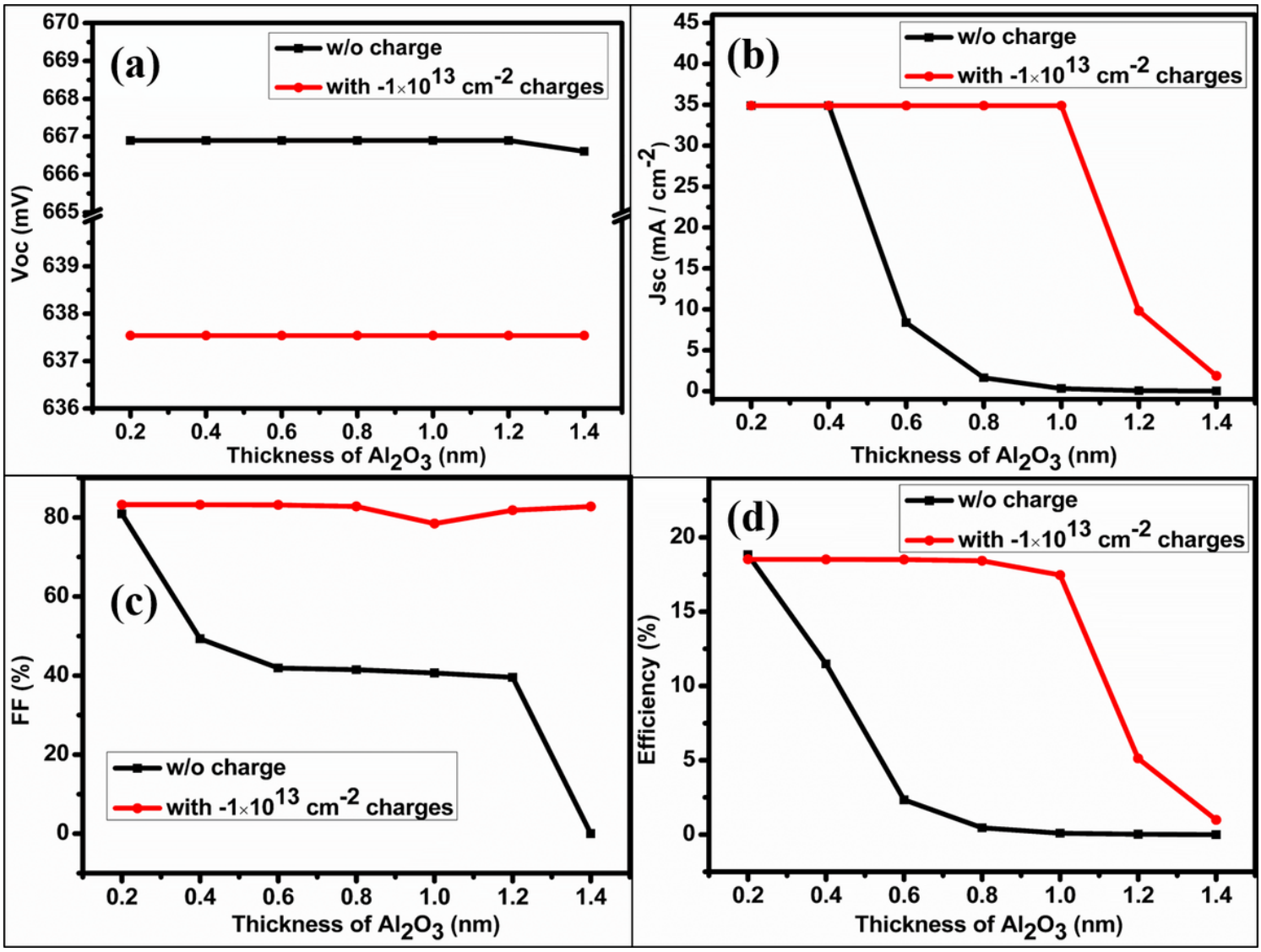

Figure 3

Influence of Al2O3 thickness on simulated HJ cell's output parameters. Bandgap, interface charges and interface defect density were fixed at 6.4 eV, -1013 cm-2 and 1011 cm-2, respectively.

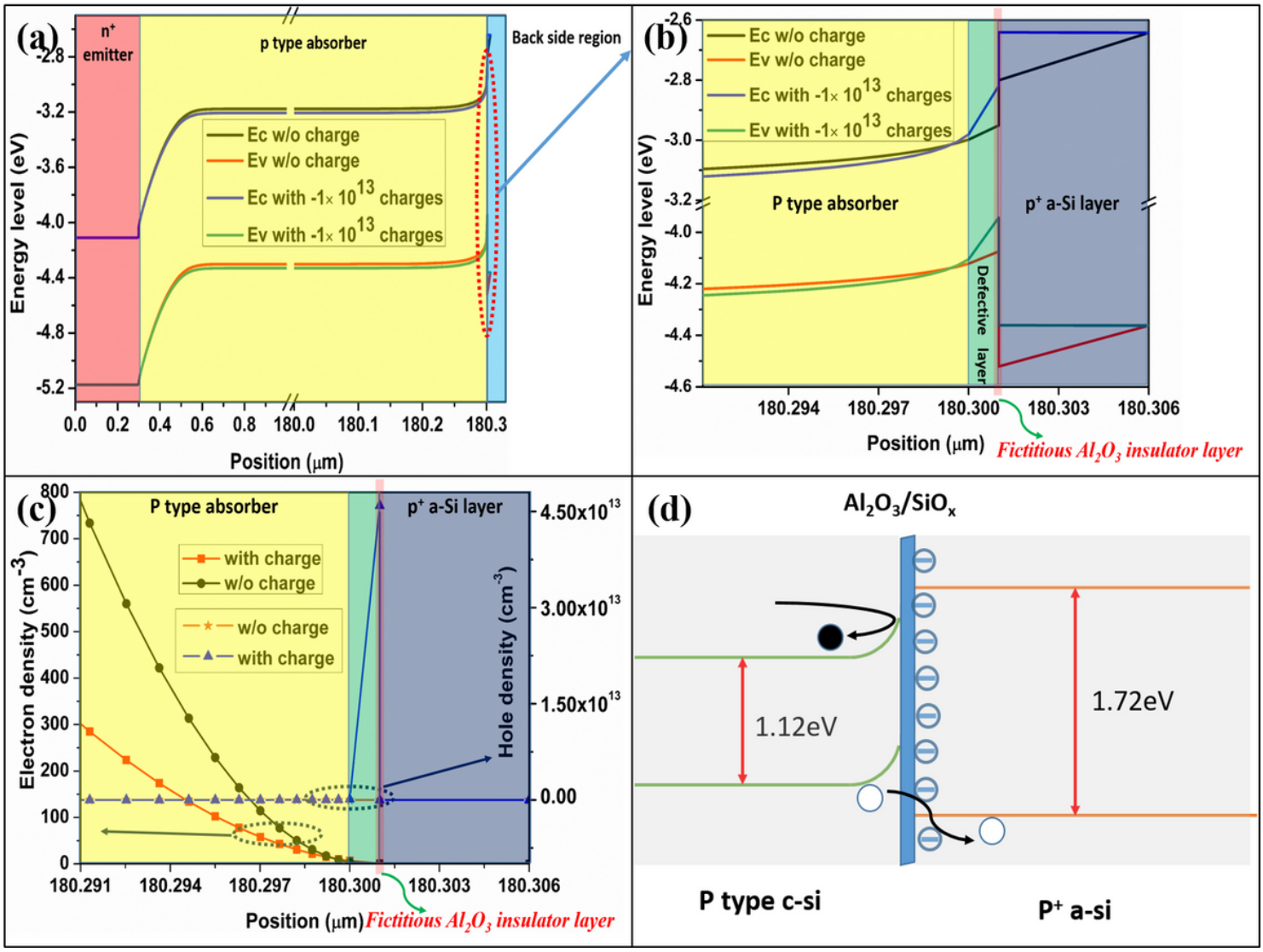

Figure 4

(a) Calculated band diagram for the entire simulated cell; (b) band diagram of enlarged backside in the simulated cell; (c) carrier density changing with position in the enlarged backside of the simulated cell; (d) schematic band diagram illustrating how the charged Al2O3 layer affecting the transport behavior of electrons and holes.

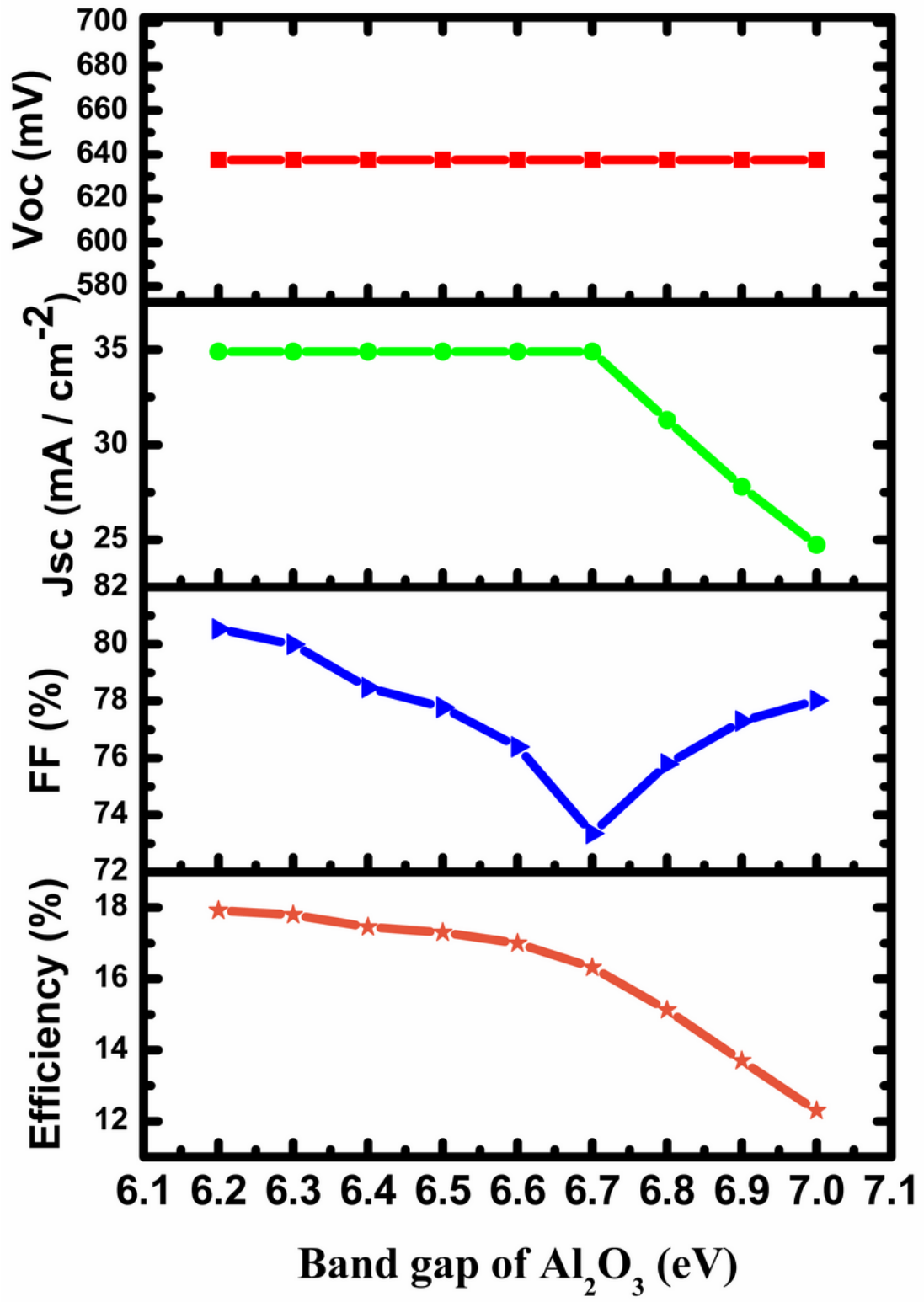

Figure 5

Influence of Al2O3 bandgap on simulated HJ cell's output parameters. The thickness of Al2O3, interface charges and interface defect density were fixed at 1 nm, -1013 cm-2 and 1011 cm-2, respectively.

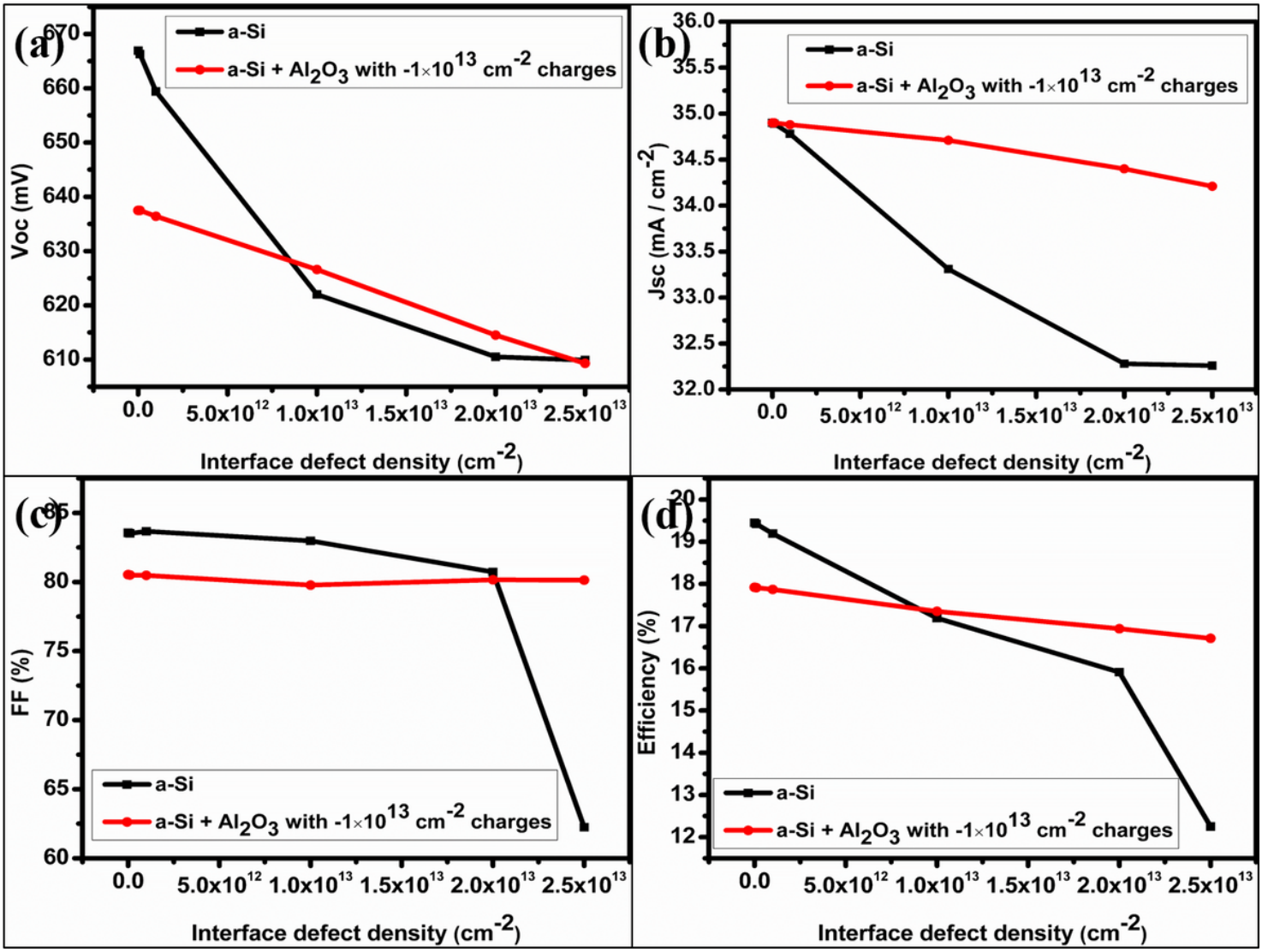

Figure 6

Simulated HJ cells' output parameters versus interface defect density (Dit). Bandgap and the thickness of Al2O3 were fixed at 6.2 eV and 1 nm, respectively.

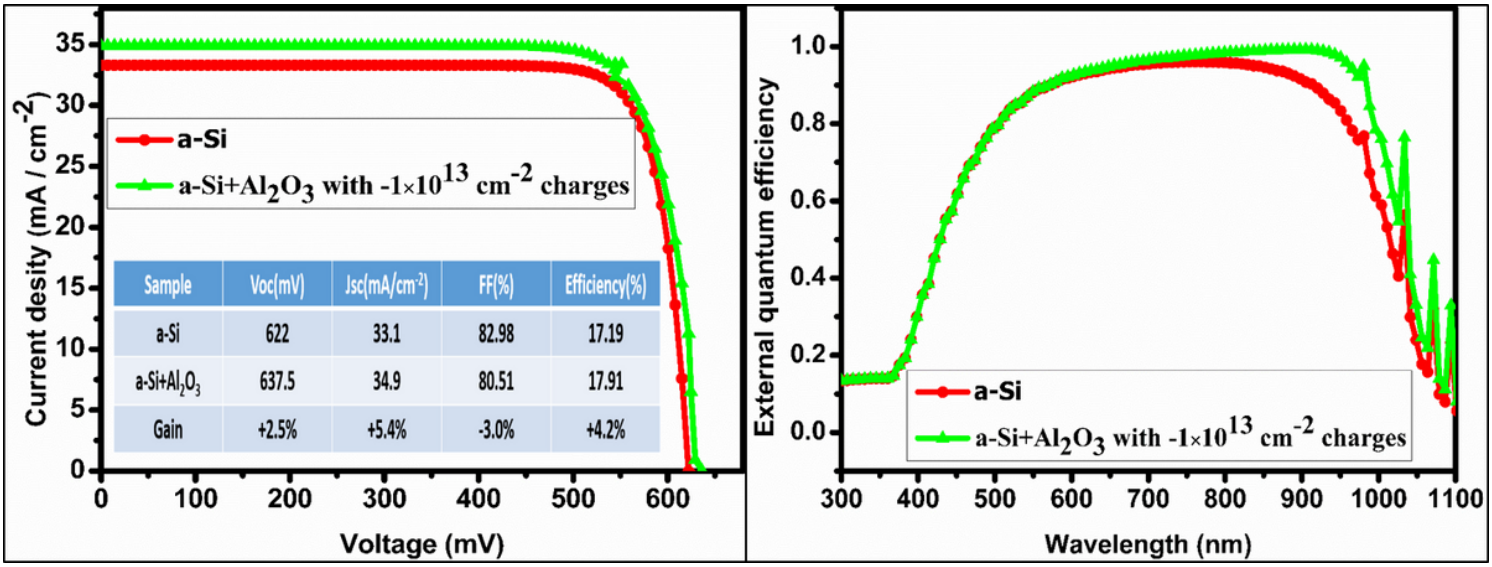

Figure 7

(a) Comparison of the I-V characteristics of a simulated cell with only a-Si and with a-Si plus Al2O3 (Qit = -1×1013 cm-2) at c-Si/p+ a-Si interface, the inset table shows the detail of both simulated cells and (b) the external quantum efficiency (EQE) of a simulated cell with only a-Si and with a-Si + Al2O3 (Qit = -1×1013 cm-2) at c-Si/p+ a-Si interface.

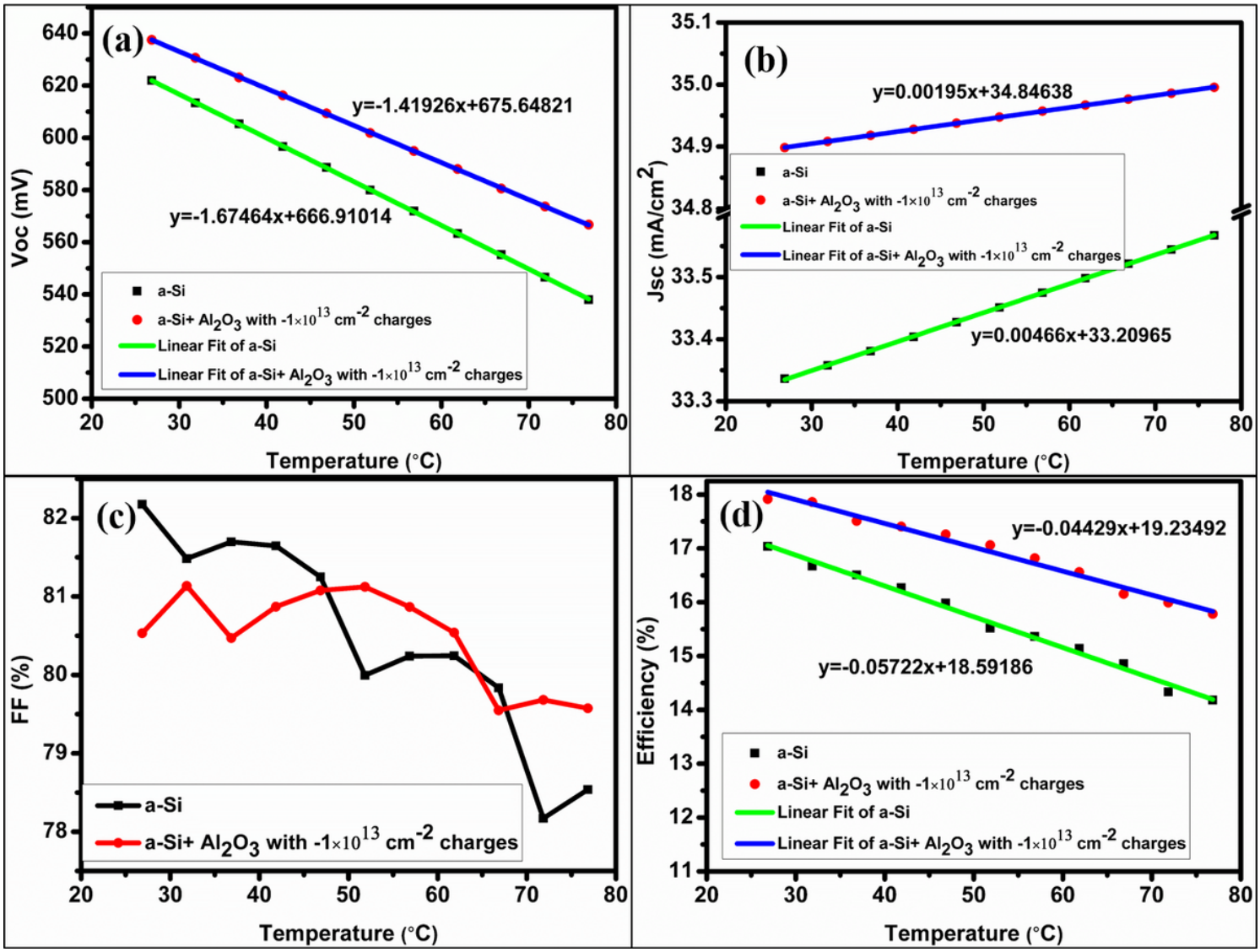

Figure 8

The temperature dependence of (a) Voc, (b) Jsc, (c) FF and (d) efficiency.